Physica Scripta

High-intensity laser experiments with highly charged ions in a Penning trap

To cite this article: S Ringleb *et al* 2022 *Phys. Scr.* **97** 084002

Physica Scripta

PAPER

High-intensity laser experiments with highly charged ions in a Penning trap

S Ringleb[1], M Kiffer[1], N Stallkamp[2], S Kumar[3], J Hofbrucker[1], B Reich[4], B Arndt[5], G Brenner[6], M Ruiz-Lopéz[6], S Düsterer[6], M Vogel[2], K Tiedtke[6], W Quint[2,4], Th Stöhlker[1,2,7] and G G Paulus[1,7]

[1] Friedrich-Schiller-Universität Jena, 07743 Jena, Germany
[2] GSI Helmholtzzentrum für Schwerionenforschung, 64291 Darmstadt, Germany
[3] Inter-University Accelerator Centre, 110067 New Delhi, India
[4] Physikalisches Institut, Ruprecht Karls-Universität Heidelberg, 69120 Heidelberg, Germany
[5] Goethe Universität Frankfurt, 60323 Frankfurt, Germany
[6] Deutsches Elektronen-Synchrotron, 22607 Hamburg, Germany
[7] Helmholtz-Institut Jena, 07743 Jena, Germany

E-mail: stefan.ringleb@uni-jena.de

OPEN ACCESS

RECEIVED
8 February 2022

REVISED
18 May 2022

ACCEPTED FOR PUBLICATION
20 June 2022

PUBLISHED
4 July 2022

Keywords: penning trap, non-linear ionisation, free-electron laser, high-power laser, ion cloud, highly charged ions

Abstract

We have conceived and built the HILITE (High-Intensity Laser-Ion Trap Experiment) Penning-trap setup for the production, confinement and preparation of pure ensembles of highly charged ions in a defined quantum state as a target for various high-intensity lasers. This enables a broad suite of laser-ion interaction studies at high photon energies and/or intensities, such as non-linear photo-ionisation studies. The setup has now been used to perform experiments at one such laser facility, namely the FLASH Free-Electron Laser at DESY in Hamburg, Germany. We describe the experimental possibilities of the apparatus, the results of the first measurements and future experiments at other laser facilities.

1. Introduction

The invention of the chirped pulse amplification (CPA) [1] to achieve extremely high laser-pulse energies opened up a large playground to study laser-matter interaction and also gave rise to new approaches concerning laser-accelerated particles [2]. The non-linear interaction of neutral atoms with lasers typically takes place in the intensity regime around 10^{14}W cm^{-2}. In this intensity regime, several effects beyond were discovered, such as Above-Threshold Ionisation (ATI) [3, 4], Non-Sequential Double Ionisation (NSDI) [5] and the High-Harmonic Generation (HHG) [6, 7]. All these effects concern the interaction of the laser field with the active electron and consider the influence of the parent nucleus. Currently, laser systems are in operation allowing intensities of the order of 10^{20}W cm^{-2} to 10^{21}W cm^{-2} [8–10]. In this intensity region, the ionisation of neutral xenon up to Xe^{20+} was reported [11] and it is possible to even further ionise hydrogen-like neon ions. In the regime of moderate laser intensities, the ADK-theory [12] is commonly used to calculate the ionisation rate. At higher ion charge states and hence higher laser intensities theories which consider relativistic effects have to be used [13, 14].

Laser pulses with high photon energy ranging in the XUV and x-ray range are typically delivered by free-electron lasers (FEL), such as FLASH in Hamburg [15, 16]. To investigate the interaction of such photons, it is feasible to use moderate intensities in comparison to CPA laser systems. Then the laser electric field is much smaller than the electric field of the nucleus at the position of the electron, the electron wave functions are only weakly perturbed and the interaction can be described by non-perturbative approaches. Theory predicts here on the one hand positive giant resonances at specific photon energies characteristic for each particle and also dips where the ionisation cross section drops by several orders of magnitudes—the so-called Cooper minima [17]. There is typically only a slight dependence on the photon energy expected for other photon energies. Tunable undulators installed at FEL laser facilities allow to study the photon energy dependence. Madsen *et al* published a

scaling law based on dipole approximation for hydrogen-like ions in high-photon energy fields [18]. Here, the cross section for a n-photon laser ionisation process ($\sigma^{(n)}$) for a particular hydrogen-like ion with nuclear charge Z and photon energy $\hbar\omega$ follows: $\sigma^{(n)}(Z,\omega) = Z^{-4n+2}\sigma^{(n)}(1,\omega Z^{-2})$. This dependence was measured with different ion targets with appropriate photon energy [19]. While in most cases the agreement with theory was good, in other cases the discrepancy was a few orders of magnitude [20]. The used targets were either in the gas phase or a solid target. This causes contributions by the more weakly bound electrons or restricts the usable laser parameters with respect to laser intensity or photon energy.

Using highly charged ions instead of neutral atoms or molecules has the big advantage of the clean configuration of a laser pulse interacting with a single active electron (typically H-like, Li-like or Na-like ions). In this case, electron-electron interactions play only a minor role or can be neglected. The results of the interaction (emitted electrons or photons) can then be attributed to this particular electron. In addition, the laser parameters can be chosen widely, because the interaction of another (more strongly bound) electron will require a laser intensity which is an order of magnitude higher than the electron of interest.

To produce highly charged ions, Electron-Beam Ion-Traps (EBIT) [21] are available as compact ion source. In such EBITs photo-ionisation experiments have been performed with highly charged ions and ionisation cross sections and resonance energies have been measured precisely [22]. This device is capable of producing ions in a high charge state in a sufficiently high quantity, however, the ion cloud inside consists of several charge states. Inside a Penning trap instead, targets of highly charged ions of a single charge state are prepared with a well-defined shape and ion density which can increase the precision of the determination of absolute ionisation cross sections. The Penning trap HILITE (High-Intensity Laser-Ion Trap Experiment) [23] is designed in a transportable fashion allowing for the combination with various laser facilities and thus a broad range of laser configurations [23]. The setup is equipped with an EBIT ion source which is capable of delivering bunches of roughly 10^6 ions with an ionisation energy up to about 1keV, for example Ar^{16+}, at a repetition rate of 1 Hz.

In this publication we will first give a brief overview of the interaction of high-intensity and high photon-energy laser pulses with ionic targets and describe the methods used for the ion target preparation. As the ion cloud typically has dimensions of about 100 μm finding the overlap of the laser focus and the ion cloud may be challenging. This issue is discussed in chapter 3. The experimental device is described in detail including the ion detection techniques to characterise the ion trap content. The achieved storage time of the ions is given. After commissioning of HILITE at GSI in Darmstadt, we have moved the complete setup to the FLASH laser facility in Hamburg to perform experiments with high-energy photons and stored ions. In chapter 4, we will give a short overview of the results and the challenges we faced. From the outcome of this first beamtime, we have identified several points to be updated for upcoming experiments which are described in section 5.

2. Non-linear laser-ion interaction

The interaction of single particles, such as atoms, molecules or (molecular) ions with laser radiation at high laser intensity is a non-linear process, as the ionisation probability increases drastically with increasing intensity I. The model which describes the ionisation process best, depends on the ratio between the photon energy of the incident laser pulse and the energy an electron gains due to the electric field strength of the laser which is represented by the ponderomotive energy U_p [24]:

$$U_p \propto I \cdot \lambda^2. \tag{1}$$

Obviously, the ponderomotive energy is high at high laser intensities and low photon energy, i.e. a long wavelength λ.

The non-linear laser ionisation process is divided into two regimes. At strong fields (high laser intensities) the electric field of the laser is comparable to the electric field caused by the nucleus at the position of the bound electron. The electric field of the laser bends the electric field of the nucleus (see figure 1), such that field ionisation can occur. If the photon energies ($\hbar\omega$) are comparable to the binding energy of the electron, the ionisation is described by the simultaneous absorption of several photons at once. To distinguish between both processes, the Keldysh-parameter [25]

$$\gamma = \frac{\hbar\omega}{U_p} \tag{2}$$

has been introduced. If $\gamma \ll 1$ the ionisation can be described in the strong field ionisation regime and if $\gamma \gg 1$ the ionisation is described in the non-perturbative regime.

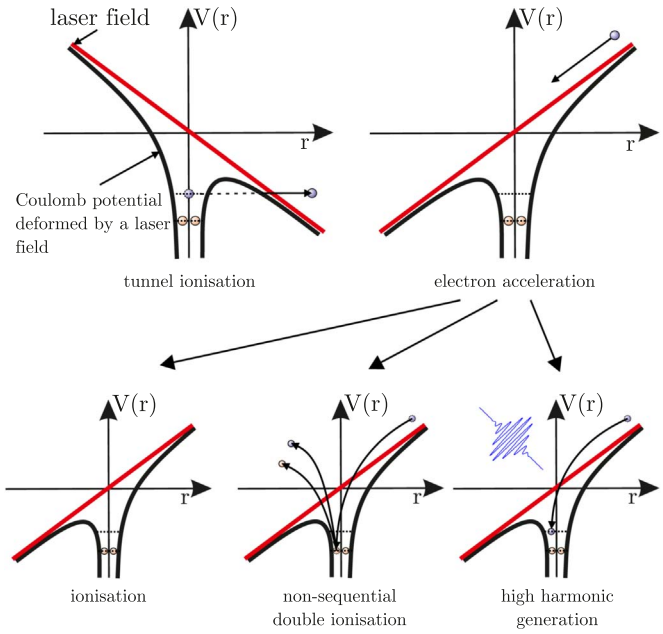

Figure 1. Different effects with high-power low photon-energy lasers. The potential of the nucleus is bent by the laser electric field. The electron tunnels through the reduced barrier and is afterwards accelerated in the electric field. At the end of the pulse the ion is ionised, when the electron is removed completely from its parent nucleus. The electron can also eject another electron by electron-impact ionisation or recombine with the ion and emit a high-energy photon.

2.1. Interaction in the strong-field regime ($\gamma \ll 1$)

The electrons of ions and atoms are bound strongly with a binding energy of about 10 eV for neutral particles up to the range of keV for highly charged ions. This binding energy can be overcome by strong laser fields in order to emit an electron from its parent nucleus. This emission of an electron can result in three possible scenarios:

(i) further ionisation

(ii) non-sequential double ionisation

(iii) emission of a high-energy photon

Ionisation of an ion means an excitation of an electron to the continuum without coming back to its parent nucleus. Depending on the laser parameters the electron's direction of flight and kinetic energy will have a certain distribution. In particular, the flight direction after ionisation will change from perpendicular to the propagation direction at low intensities to forward direction at relativistic intensities [26]. The ionisation rate is typically calculated using ADK-theory [12]. This theory is developed for non-relativistic intensities up to 10^{16}W cm^{-2}, but was also found to be still valid beyond this intensity [27]. In contrast, Milosevic *et al* [14] presented calculations which predict a drop of the ionisation rate considering relativistic effects beyond 10^{19}W cm^{-2} while Popov *et al* [13] predict an enhancement.

The effect of non-sequential double ionisation was reported initially with xenon and neon ionised by moderate intensities of the order of 10^{12}W cm^{-2} to 10^{13}W cm^{-2} [28] and is explained by the ejection of a second electron by electron impact ionisation by the returning electron. Since at high intensities the initial electron is accelerated along the laser propagation direction away from the ion, the probability for electron impact ionisation decreases. Nevertheless, this effect could be observed up to intensities around 10^{18}W cm^{-2} with methane as target [29]. In that experiment the influence of all active electrons had to be considered in the data evaluation. Using for example lithium- or sodium-like ions as target, there is only one active electron interacting with the laser which allows for direct data analysis.

The generation of photons with an energy of odd multiples of the incident photon energy E_{ph} - high harmonic generation—is explained by the recapture of a previously ionised electron by its parent nucleus. During the interaction with the laser field it gains energy which is then emitted as a photon. The highest possible harmonic order (n_{max}) is defined by the so-called cut-off and is typically approximated by [7]

$$n_{\max} \cdot E_{ph} = 1.32 \cdot I_p + 3.17 \cdot U_P, \tag{3}$$

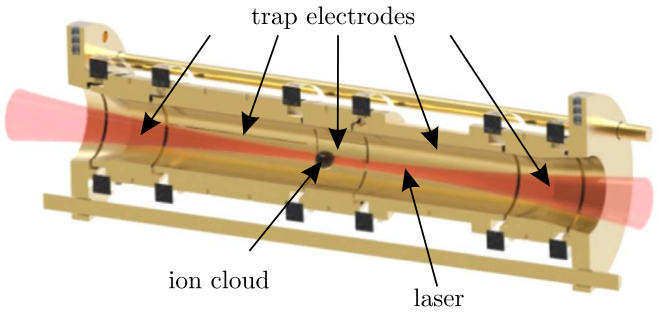

Figure 2. Working principle of the HILITE Penning trap. A compact ion cloud is stored in the trap centre and is irradiated by a high-intensity laser pulse.

where I_P is the binding energy of the electron. At high intensities, this will allow for the generation of high-energetic photons in the high keV regime. The efficiency of the HHG production will be limited by the forward propagation of the relativistic electrons.

2.2. Interaction in the high photon energy regime ($\gamma \gg 1$)

If the binding energy of the electron in a highly charged ion is higher but close to the photon energy of the laser, there is a certain ionisation probability that several photons are absorbed at once. The ionisation rate w for the simultaneous absorption of k photons in this regime can be expressed by:

$$w = \sigma_k I^k, \tag{4}$$

where I is the laser intensity and σ_k is the ionisation cross section for a certain ionisation path. As the electric field strength of the laser is much lower than the electric field of the ion's nucleus at the position of the bound electron, perturbative approaches are used to calculate the ionisation cross section σ_k. It depends strongly on the number of absorbed photons and is otherwise typically only slightly dependent on the photon energy.

3. The Penning trap setup and ion target preparation

For laser-ion interaction experiments we use ensembles of highly charged ions to increase the number of interacting particles. They are stored in the trap centre and prepared for the interaction with a focussed intense laser pulse. The principle is shown in figure 2. Here, the ions are described as non-neutral plasma, taking the interaction of the ions with each other into account. The plasma-parameter Γ is introduced as [30]

$$\Gamma_P = \frac{q^2}{4\pi\epsilon_0 a_{ws} k_B T}, \tag{5}$$

where q is the charge of an individual ion, k_{BT} the thermal energy of the ions and a_{ws} the effective ion-ion-separation. If the condition $\Gamma \gtrapprox 2$ is fulfilled, the ion cloud can be recognised as strongly correlated and performs a strongly coupled motion inside the trap. The shape of the ion cloud is then always an ellipsoid of revolution with a characteristic length and radius which can be controlled by the trapping parameters (magnetic field strength B and trapping potential U_0). Typically, this motion is driven actively by the application of a rotating dipole field which allows the direct control of the ion density and the ion cloud shape [31]. The procedure to calculate the ion cloud shape from the trapping parameters is well described in [32]. The maximum achievable ion density n_{max} is limited by the ion mass m and the magnetic field strength. This is the so-called 'Brillouin-Limit' given by

$$n_{\mathrm{max}} = \frac{\epsilon_0 B^2}{m}. \tag{6}$$

For ion ensembles with a kinetic energy of about 0.5 meV which corresponds to an ion temperature of 4 K the ion density is constant over the whole ion cloud and drops at the edges. Ensembles with higher kinetic energy have a larger region of smaller ion density at the edges. The reliable prediction of the ion cloud dimensions, density and shape will also allow for the measurement of absolute cross sections.

To reach the maximum possible ion density, efficient cooling is necessary which may take several seconds up to minutes. The trap can also be driven in a fast ion-load mode without cooling which reduces the ion density by a few orders of magnitude though, but laser ionisation experiments can be performed with a repetition rate of 1 Hz—10 Hz instead.

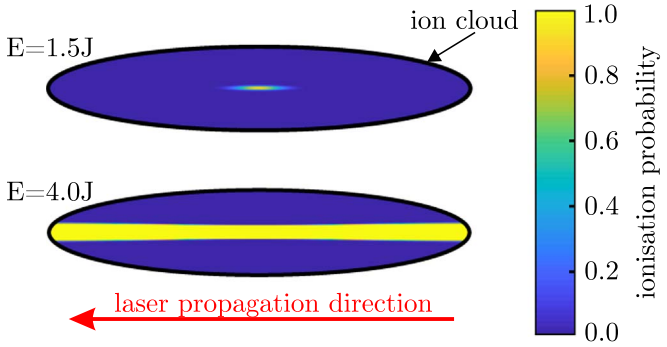

Figure 3. Ionisation probability distribution inside the ion cloud. For low intensities (upper) the ionisation takes place in the cloud centre. In the case of high intensities (lower) the ion yield is limited by the axial extension of the ion cloud.

3.1. Overlap of laser and ion cloud

One crucial exercise in the combination of highly charged ions with a high-power laser is to find the overlap of the laser waist and the ion cloud. In the case of 1000 hydrogen-like oxygen ions (O^{7+}) a typical axial and radial extend of the ion cloud is 200 μm and 50 μm, respectively. Depending on the focussing parameters, a high-power laser has typically a focal spot diameter of roughly 10 μm. In this configuration, a well-centred laser with respect to the ion cloud has interaction partners over its whole radial extend. In axial direction instead, the interaction region is limited by the length of the ion cloud. Figure 3 shows the ionisation probability inside the ion cloud calculated for a cloud of 1000 O^{7+} ions. The laser is assumed to be a titanium:sapphire laser with a pulse duration of 20 fs focussed by a f/10 parabolic mirror. In the lower image the pulse energy is 4 J which corresponds to a maximum laser intensity of $I=1 \cdot 10^{19}$W cm^{-2} in the laser focus. Increasing the pulse energy further the region where the laser intensity exceeds the ionisation threshold is extended to the frontier of the ion cloud. Hence the number of ionised particles does not rise further by increasing the laser pulse energy.

The number of ionisation events N_{ion} of a particle with nuclear charge Z and charge state q is a convolution of the spatial intensity distribution I(r,z) and the intensity-dependent ionisation probability P given by:

$$N_{ion} = \pi \cdot n \cdot \int_{-z_0}^{+z_0} \int_{0}^{r_0} r \cdot P(Z, q, I(r, z)) \mathrm{d}r\mathrm{d}z. \tag{7}$$

The ion cloud is assumed to have a homogeneous ion density n and the limits of the integral are the edges of the ion cloud in axial and radial direction z_0 and r_0, respectively. The intensity distribution around the laser focus can be measured in the experiment and the ionisation probability can be taken from the used ionisation model. Using now several charge states and laser intensities, the model can be tested by the comparison of the prospected ion yield and the measured.

To find the ideal overlap between the laser and the ion cloud, the position of the laser focus is varied in axial and lateral direction and the number of ionisation events is monitored. As the position of the ion cloud is fixed by the trapping parameters and hence reproducible, the position of the maximum ionisation results can be assumed to be the ideal overlap for all following measurements.

In contrast to such single-shot experiments, an ion trap confines the ions of interest for several seconds and even minutes at one spot, depending on the background pressure. This allows for accumulating several laser pulses with the very same ion target using for example a high repetition laser. For example, in case of O^{7+} with the laser and trap parameters above, we will produce approximately 30 O^{8+}-ions per minute, if the ionisation probability is 1/1000.

3.2. The HILITE Penning trap setup

In a Penning trap ions of several charge states can be stored at once which enables the simultaneous storage of laser-ionisation educts and products. A Penning trap is the superposition of a static electric and magnetic field which allows for axial and radial confinement of charged particles, respectively. This trap design is very rigid and the storage of particles with high energy is possible, especially when accelerated by high-power lasers. The magnetic field is typically created by a superconducting magnet and a set of at least three electrodes. At HILITE the maximum achievable magnetic field strength is 6 T. The open-endcap design depicted in figure 2 of the electrodes allows the injection of externally produced highly charged ions and a tight focussing of high-power lasers with a full opening angle of up to $\alpha = 11°$ which corresponds to an aperture of f/5.2. A detailed description of the trap electrode configuration can be found in [33]. The complete setup shown in figure 4 has an overall footprint of 4 m $\times$ 1.5 m with a height of about 2m. The ion trap is loaded by an external ion source with

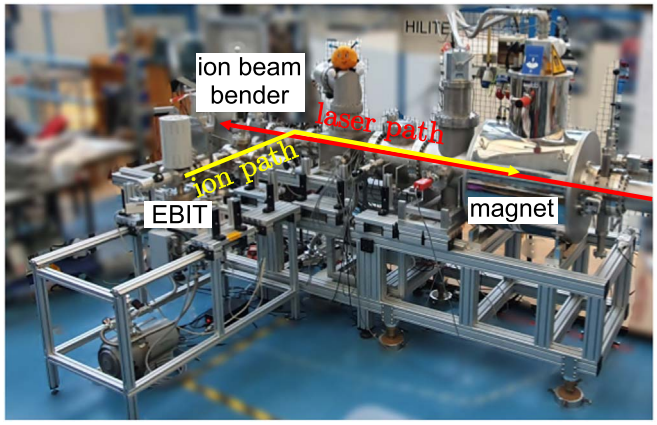

Figure 4. The complete HILITE setup with a dedicated source for highly charged ions (EBIT), ion deflector and superconducting magnet which contains the trap electrodes.

a Wien-filter which transmits only ions with a defined charge-to-mass ratio. A 90° electrostatic ion deflector aligns the incoming bunches with the axial direction of the laser beam and the ion trap. This enables the setup to be transparent for the laser beam.

3.3. Dynamic ion capture

The ions for the laser-ion interaction are produced by a dedicated EBIT ion source from DREEBIT [21]. The ions are extracted in single bunches with a kinetic energy of typically 1-2 keV/q. The number of ions in a single bunch depends on the charge state and is typically between 10,000 and 100,000. Also the production rate depends on the ion species. Typical breeding times are about 10 ms for doubly charged particles and 1000ms for the highest charge states of light ions. The transport of the ions from the EBIT to the ion trap is a crucial part of the ion target preparation. As the ion trap is only capable of capturing ions up to an energy of 200 eV/q the ions hence have to be decelerated first. This is accomplished by a dedicated pulsed drift tube close to the trap centre. With appropriate choice of deceleration parameters we have achieved axially compressed, decelerated ion bunches.

The ion bunch properties, such as kinetic energy, ion number and bunch length can be deduced from the charge-counter signal shown in figure 5(b) (blue curve) by the evaluation of the plateau amplitude U_{plat}, the area below the signal and the slope of the rising edge. The detailed procedure to obtain these quantities is described in [34]. With this procedure, we have been able to obtain a kinetic energy of the ion bunch below 100 eV/q and an axial extension of less than 50 mm. These ion bunches are then captured by time-sensitive fast electrode switching. With this technique we have captured several thousands of ions at once and stored them for minutes.

3.4. Target preparation techniques

The characterisation of the interaction educts before the laser-ion interaction is done using non-destructive ion-detection techniques. The Fourier-Transform Ion Cyclotron Resonance (FT-ICR) technique is a well-developed method in Penning traps, is capable of detecting low as well as large ion numbers, and is used in the HILITE Penning trap [35]. To achieve single-species ion clouds the so-called SWIFT-technique can be used to remove unwanted ion species by resonant ion excitation [36].

The ions initially have a high kinetic energy after ion capture and hence have to be cooled to an energy in the sub-meV regime. Resistive ion cooling is the established technique in Penning traps and is applied at HILITE [37].

The electrodes are held at a temperature of 4 K and allows for a low background pressure due to cryogenic pumping and a storage time of several minutes. Keeping the ions at a certain position for a long time enables us to accumulate several hundreds to millions of laser pulses with the same ion targets, depending on the laser repetition rate. This becomes necessary close to minima in the ionisation cross section. At a high ionisation cross section instead, the ion target may be depleted with a single or a few laser shots and has then to be renewed.

3.5. Ion species determination

Although we capture only one isolated charge state from our ion source in the trap, we expect to gain several other ion species from residual gas ionisation events by charge exchange and reactions. In order to obtain the ion-lifetime constant and the evolution of the content inside the ion trap, we use a destructive detection method. This has the advantage, that we can characterise the whole ion trap content. Therefore, we open the trap and eject all ions towards a time-sensitive microchannel-plate (MCP) detector at once. To further accelerate the ions, we

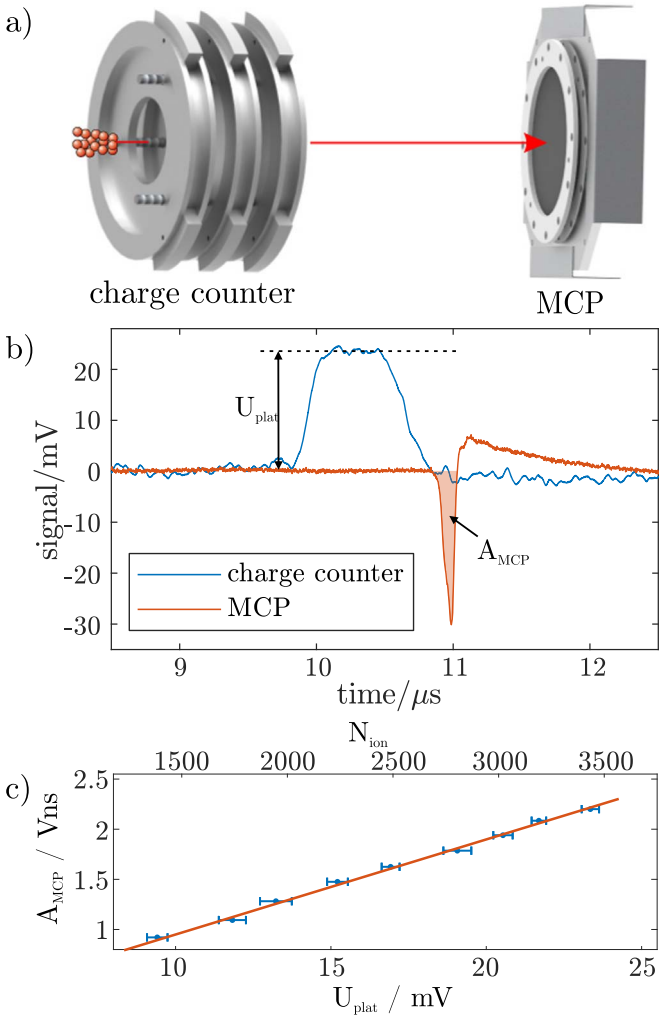

Figure 5. (a) The destructive ion detection is calibrated using a single-pass non-destructive charge counter. (b) To determine the number of ions with the MCP detector the area below the MCP signal is used. (c) The area below the MCP is proportional to the number of ions.

have applied an offset voltage of 50 V to all storage electrodes. So all ions have had an initial energy of at least 50 eV/q which reduced the influence of the individual kinetic energy of each ion. We have recorded the individual time of flight for each ion species. The prospected time of flight of a particular mass-to-charge m/q starting at position z_0 with a kinetic energy $E_{kin,0}$ to the detector positioned at z_{end} is given by

$$t_{tof} = \sqrt{\frac{m}{q}} \int_{z_0}^{z_{end}} \frac{\mathrm{d}z}{\sqrt{2(U(z_0) - U(z) + \tilde{E}_{kin,0})}}. \tag{8}$$

This formula is deduced from the conservation-of-energy law with a calculated electric potential U(z) of the electrodes. As the initial potential energy of 50 eV/q is much higher than the initial kinetic energy and since all ions start approximately at the same position, the integral in equation (8) is constant for all trapped ions. Consequently, we expect a linear dependence between time of flight and the square root of the mass-to-charge ratio. Figure 6 shows the time-of-flight spectrum of the ejected ions after different storage times of 30 s, 3 min, and 20 min. Here, doubly charged carbon (C^{2+}) was captured initially. At a time of flight of about 8.6 μs the remaining ions of the captured species can be found. Additionally, peaks can be found which correspond to other ions created from the residual gas by charge exchange . In this particular measurement, the background pressure was poor by design and a lot of different ion species and even molecular ions have been formed inside the trap. This allowed us to develop and test a procedure to determine the ion species from the ions' time of flight. For each peak we have extracted the ions' time of flight and have assumed the very first peak to be the ion species with the lowest possible mass-to-charge ratio - H^+. Then we have assigned a reasonable mass-to-charge ratio and hence a reasonable ion species to each peak. Table 1 summarises the ion species found. Plotting now the time of flight over the square root of the assigned mass-to-charge ratio, we have found a linear dependence according to equation (8). Only the initially captured C^{2+} ions and the C^+ ions created via charge exchange are

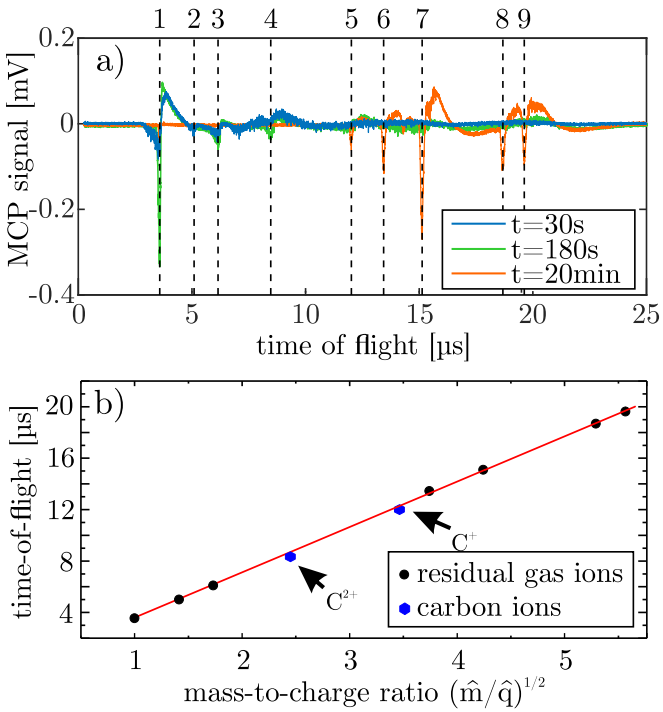

Figure 6. (a) Time-of-flight spectra after different ion storage times. The initially trapped C^{2+} ions interact with the residual gas creating other ion species. The indices mark different ion species and correspond to the entries in table 1. (b) Plot of time of flight versus m/q in units of u/e.

Table 1. Summary of the time-of-flight (tof) spectrum and the corresponding ions. The mass-to-charge ratio (m/q-ratio) is given in terms of atomic mass unit / elementary charge.

	tof / μs	m/q-ratio	ion
1	3.55	1/1	H^+
2	5.00	2/1	H_2^+
3	6.10	3/1	H_3^+
4	8.45	12/2	C^{2+}
5	12.00	12/1	C^+
6	13.44	14/1	N^+
7	15.10	18/1	H_2O^+
8	18.68	28/1	CO^+
9	19.63	31/1	HNO^+

below the linear fit function which can be assigned to the remaining kinetic energy from the ion capture procedure. This proves our ion assignment procedure to be a robust method for obtaining the ion species stored in the trap.

3.6. Ion storage time

The ion storage time is mainly limited by charge exchange with residual gas. This on the one hand reduces the number of ions of interest and on the other hand increases the number of ions polluting the interaction region. So, the background pressure has to be kept low in order to prepare a pure single species ion cloud.

The measurement of the background pressure is performed indirectly using the lifetime constant of the ions. From the time signal at the MCP we deduce the number of extracted ions, as the area below the signal is directly proportional to the number of ions. We have proven this dependence with a non-destructive single-pass charge counter whose signal height (U_{plat}) is known to be linearly dependent on the number of particles as well [34]. To determine the time-dependence of the number of stored ions, we have acquired a time-of-flight spectrum each 30s, evaluated the evolution of the C^{2+} - signal (see figure 7(b)) in the time-of-flight spectrum and obtained the time evolution of the relative number of ions ejected from the trapping region. From the decaying curve in

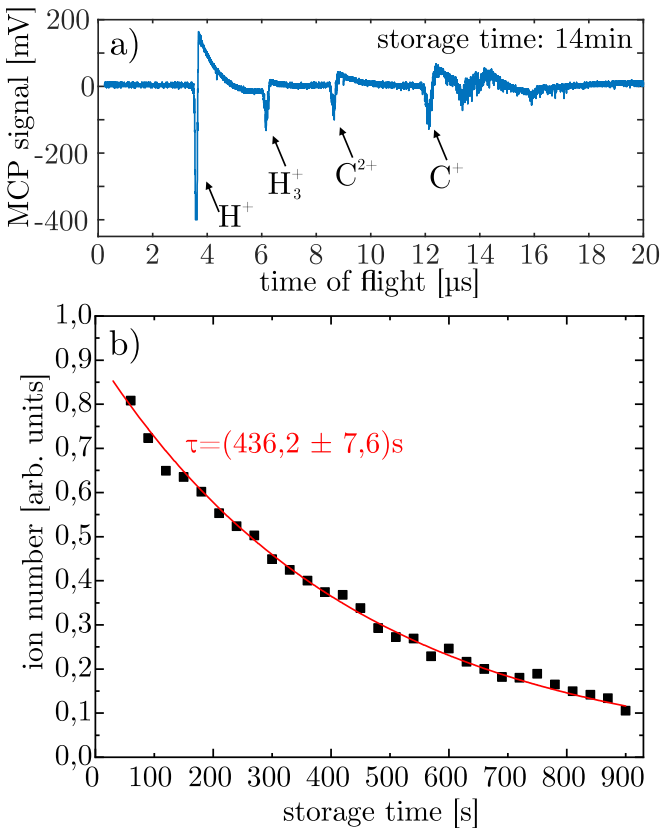

Figure 7. (a) Time-of-flight spectrum of trap content after a storage time of 14 min. The main peaks are nominated here. After the C^+ peak there are ions of other species which are not relevant to deduce storage time and residual gas pressure. The number of stored C^{2+} ions has been deduced from the area below the MCP signal. b) Dependence of the number of stored C^{2+} ions from the storage time.

figure 7(b) we obtain an ion lifetime constant of

$$\tau = (436.2 \pm 7.2)\,\mathrm{s}. \tag{9}$$

As the hydrogen peak at 3.6 μs is the highest and also the H_3^+ - peak is very prominent and appears fast (see figure 7(a) and 6), we assume hydrogen to be the dominant residual gas. So, we can deduce a background pressure of

$$p = 2.1 \times 10^{-10}\ \mathrm{mbar} \tag{10}$$

from the ion lifetime constant [38].

4. Laser beamtime at the FLASH facility

The HILITE ion trap is meant to be moved to different laser facilities. After commissioning at GSI in Darmstadt we have performed first laser experiments with trapped ions at the FLASH FEL facility in Hamburg, with the aim of measuring the dependence of the ionisation cross section of H-like carbon (C^{5+}) on the photon energy (see chapter 5.2.1).

The complete setup has been disassembled at GSI and successfully reassembled at the FLASH2 FL24 open port beamline (see figure 8). We have been able to produce, decelerate, and capture ions delivered by the EBIT. Unfortunately, the ion storage time of highly charged carbon (C^{5+}) was below 1 s. We deduced the background pressure from the ion lifetime constant and it was found to be of the order of 1×10^{-8} mbar and hence two orders of magnitude worse than in the commissioning phase at GSI. Up to now, we are not sure what the origin of the bad vacuum has been, but it has not allowed us to prepare a compact ion cloud for precise cross section measurements.

Instead we have decided to analyse the interaction of lower charged C^{2+} - ions which appeared to have a longer lifetime. To further increase the number of stored ions, we have chosen a storage time of about 50 ms. For sure, in this short time, the preparation of a well-defined ion cloud has not been possible. In this procedure, the experimental sequence was clocked by the FLASH laser pulse-train rate with a frequency of 10 Hz. The pulse duration and the laser pulse energy were 100 fs and 2.7 μJ, respectively. The laser delivered every 100 ms a pulse

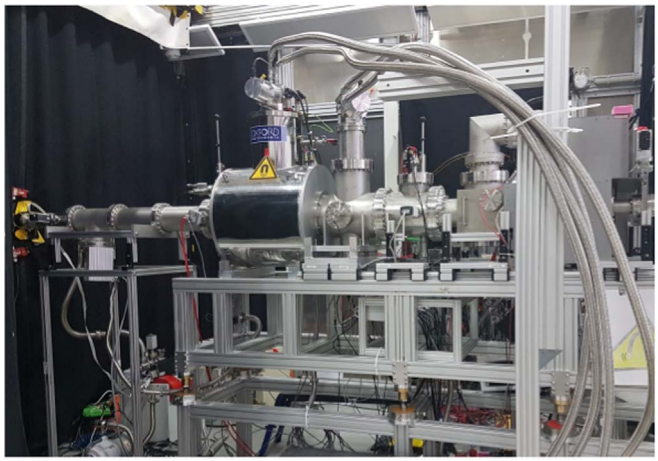

Figure 8. The HILITE Penning trap is attached to the FLASH II—Beamline FL24. The laser beam is injected from the left and is focussed to the centre of the magnet.

train of 400 XUV laser pulses with a pulse separation of 1 μs. Thus, there was a time window of 99.6 ms without laser radiation. During this time window, we have cleared the trap from remaining ions from the previous measurement and initiated the ion capture procedure using an early trigger signal. The ions then were stored for 50 ms before being ejected towards the time-sensitive MCP detector.

Since the short storage time has not allowed for cooling the captured ions, they still have had a kinetic energy of the order of 20 eV/q and hence have been distributed over about 30 mm in the axial direction. This also has resulted in a very wide distribution in the time of flight. The radial distribution is unknown. Nevertheless, we have been able to detect an ionisation process due to non-linear laser ionisation. To this end, we have recorded the timing signals of three different scenarios shown in figure 9(a): residual gas ionisation using the laser without stored ions (S_{res}), the pure ion signal without laser radiation (S_{ion}), and the signal of the ions after laser ionisation (S_{meas}). The interaction signal which shows the ionisation process (S_{int}) is then cleared with following calculation rule:

$$S_{int} = S_{meas} - S_{ion} - S_{res} \tag{11}$$

The positive interaction signal in figure 9(b) means a loss of previously stored C^{2+}-ions due to the laser irradiation. The ions were spread widely in time which can be addressed to ion heating. The reason for the heating is not understood in detail. Nevertheless, we had to be recompressed the ion bunch during ejection which led to a shift of the time-of-flight signal. We interpret the loss of C^{2+}-ions as laser-ion interaction. In consequence we expect the occurrence of ion signals for produced C^{3+}. Unfortunately, these ions could not be distinguished from the background.

An important outcome from this beamtime is the necessity to decouple the trap vacuum further from the residual gas outside of the trap electrodes. Meanwhile, we have developed a new trap with a smaller aperture of only 4 mm instead of 20 mm. This will reduce the area of the aperture by a factor of 25 and will reduce the pollution of the interaction region significantly. In order to still provide a large opening angle of about 14° we have reduced the trap length to 65.4 mm.

5. Prospective laser ionisation experiments

The use of highly charged ions with a defined quantum state as initial particles gives a very clean environment for laser-ion-interaction experiments. The techniques to produce, select and store the ions are available and well-established. The main feature is the custom-made ion target for the particular laser intensity or photon energy. For example, while at FLASH a photon energy of up to 295 eV hydrogen-like carbon (C^{5+}) or nitrogen (N^{6+}) would be suitable targets for non-linear photo ionisation, at European XFEL which delivers a photon energy of up to 25 keV, hydrogen-like xenon (Xe^{53+}) would be an appropriate candidate.

To test the theory of the interaction of particles with intense laser pulses, it is advantageous to have only a single active electron. So any interaction with the laser field can be addressed to this particular electron and any electron-electron interaction can be neglected.

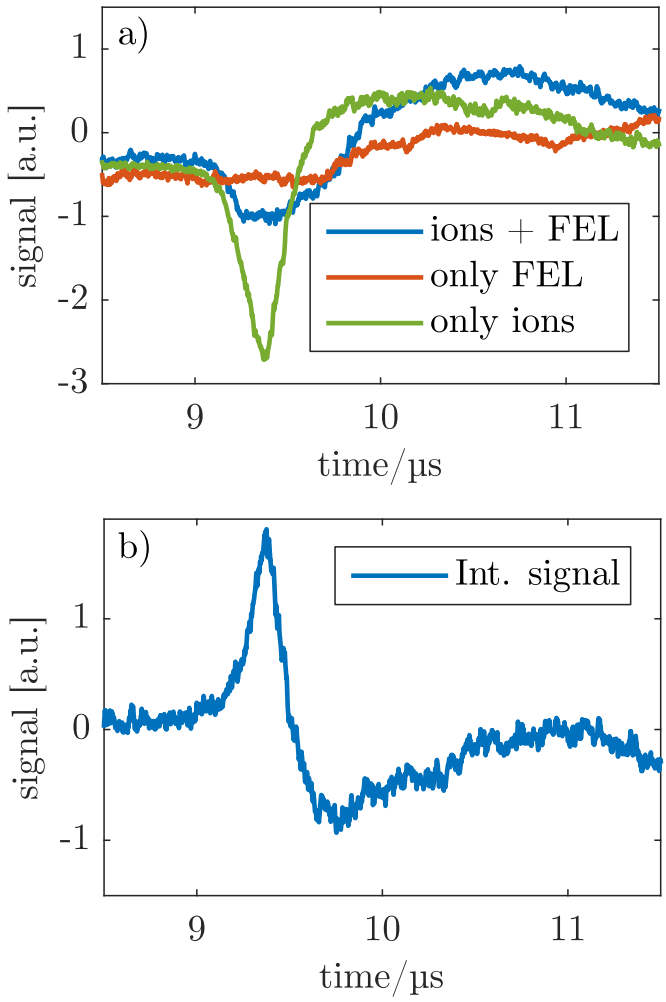

Figure 9. (a) Three recorded signals to determine the laser-ion interaction. (b) Calculated interaction signal using equation (11).

5.1. Science cases for ion trap experiments with high-power lasers

In the regime of high-intensity laser-ion interaction there have been some theoretical works predicting the ionisation rate at intensities beyond 10^{19}W cm^{-2} [13, 14, 39–41]. Electrons released with such high intensities have relativistic energies after emission and their emission angle is shifted towards the laser propagation direction [26]. By now, this effect was only measured with neutral targets and the electron signal had to be disentangled with respect to the individual charge states afterwards [42].

5.1.1. Hydrogen-like ions

Using initially highly charged ions with a single active electron, the laser-intensity dependent ionisation cross section, electron emission energy and electron emission angle will be measured. The other way around, as the ionisation cross section for low-Z hydrogen-like ions can be predicted precisely, the laser intensity in the focus can be deduced from the number of ionised particles [39].

5.1.2. Sodium-like ions (Kr^{25+} and Ar^{7+}) as laser target

Sodium-like krypton comprise several features at once. As there is only a single electron in the shell of the weakest bound electrons, one can assume this particular electron to be the only one interacting with the laser. This allows for easier theoretical treatment to predict the laser-ion interaction. Using the ADK-theory one gets an ionisation probability of 50% at an intensity of $2.7 \cdot 10^{19}$W cm^{-2}.

In case it returns to the residual ion, the high amount of residual electrons gives an increased chance for the active electron to eject one of the remaining ten electrons due to electron impact ionisation. As the laser intensity will be less than half the threshold intensity for the electrons in the L-shell as highlighted by the green region in figure 10, any ions with a charge state higher than Kr^{26+} can be assigned to NSDI. In this context, one can measure the dependence of the amount of ions produced by NSDI of the laser intensity over one order of magnitude.

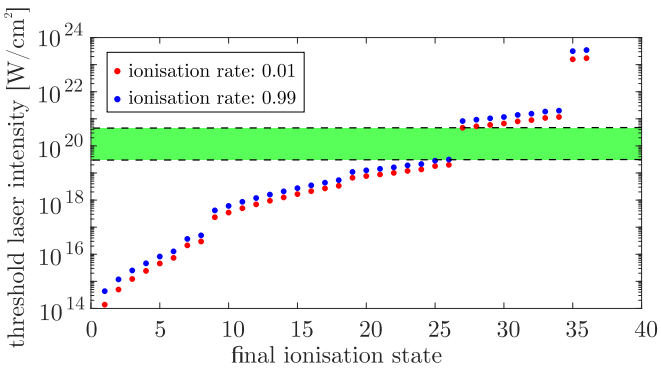

Figure 10. Threshold intensity for different charge states of krypton. The blue and red dots denote the 1% and the 99% ionisation probability, respectively. In the intensity region marked in green, the 3s electron is removed from the residual ion while the 2s electrons are not affected by the the laser at all. Here, for example the intensity dependence of ATI, NSDI or HHG can be investigated with a single active electron.

In case the active electron returns to its parent nucleus and is recaptured, we expect higher harmonics to be emitted. In this case, the gained energy is emitted as a photon with high energy. In [43] the photon energy distribution of higher-harmonics for intensities of about 10^{16}W cm^{-2} is calculated and using neutral helium as a target the generation of 1keV x-ray photons is reported. Using here Na-like argon as target with a peak intensity of about $3 \cdot 10^{16}$W cm^{-2} we expect even higher photon energies since the ionisation potential (see equation (3)) is about 0.9 keV higher. In this intensity regime the influence of the laser's magnetic field becomes relevant for the electron motion resulting in a lower number of photons. This will be investigated in planned experiments. The effect of ATI was theoretically described in [44] for hydrogen-like carbon. The authors predict 10×10^{12}electrons/s with a kinetic energy which corresponds to the 30.000th order of the fundamental photon energy of 1.55 eV. We will equip the Penning trap setup with a time-sensitive electron detector to be able to detect the electron and deduce their energy from the time of flight.

5.2. Ion trap potentials for experiments with lasers at high photon energies

In the regime of high photon energy, the particular transitions in ions can be investigated. Here, one uses that the photon energy is similar but typically lower than the binding energy of the electron.

5.2.1. Ionisation of hydrogen-like carbon

At certain photon energies resonances enhance the ionisation rate drastically where the difference between two energy levels is a multiple of the photon energy [45]. An interesting candidate here is hydrogen-like carbon, whose photon-energy-dependent ionisation cross section is depicted in figure 11. There are four prominent peaks depicted resulting from resonant two-photon-excitation with subsequent ionisation by a third photon. The peaks are separated clearly from each other and can be resolved. In the two-photon regime for photon energies above 244.8 eV no enhanced ionisation cross sections are expected rather than an almost flat behaviour. Though FEL lasers typically obey a certain spectral width, the ionisation can be treated independently from the photon energy. As the laser and ion target properties are known well, absolute ionisation cross section can be determined. This allows for a good comparison of experimental results with theory.

5.2.2. Cooper Minima in lithium-like oxygen

At certain frequencies, resonant processes depicted in figure 12(a) occur, resulting in a peak in the cross-section spectrum. This is shown in the calculation in figure 12(b) with lithium-like oxygen ions. The peak at 82 eV corresponds to a resonant excitation from the $n = 2$ to $n = 3$ level with subsequent non-resonant ionisation from the excited state.

In the region of 92 eV instead the ionisation cross section drops by several orders of magnitude. This is called the cooper minimum and can be addressed to a minimum in the matrix element between the s ground-state wave function and the wave function of the photo-ionised electron [17].

To measure low ionisation cross sections it is necessary to accumulate many laser pulses. To this end, it is important to have an ion target at a defined and constant position. An ion trap here is the only device which is able to provide a single-species ion cloud of highly charged ions.

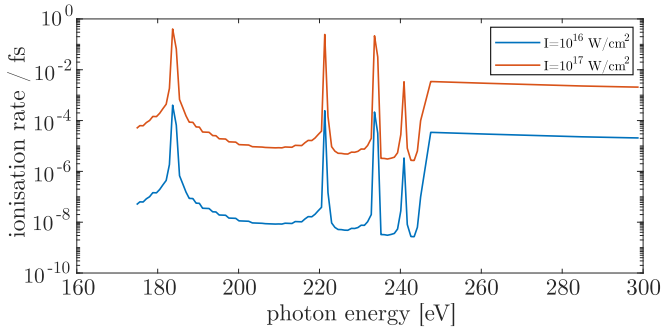

Figure 11. Dependence of the ionisation cross section of H-like carbon on the photon energy. In the three-photon absorption region there are peaks from resonant excitations while in the two-photon absorption region the cross section is almost independent from the photon energy.

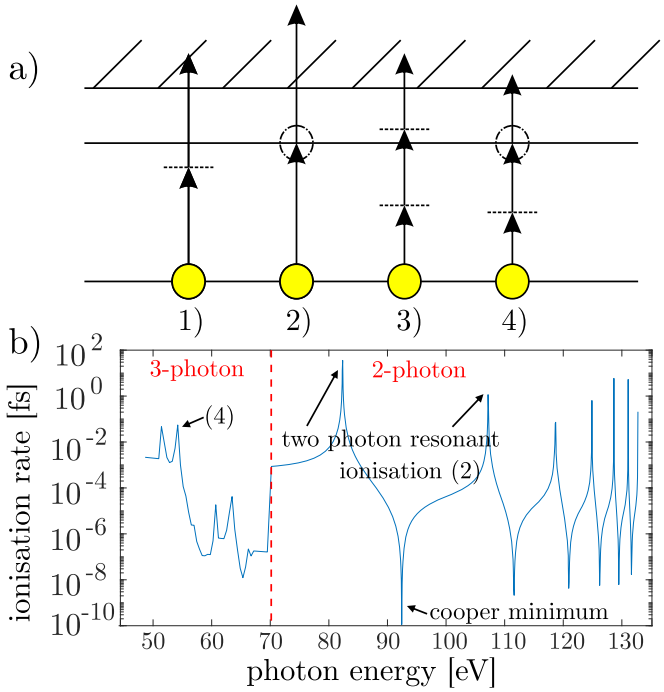

Figure 12. Photon-energy dependence of the ionisation rate of Li-like Oxygen (O^{5+}. Below 70 eV it is a three-photon process and above a two-photon process. The peaks are resonant enhancements of the ionisation rate, when die photon energy matches an inner-ion transition energy. The dips instead, occur when the dominant ionisation channel via virtual intermediate states is suppressed.

6. Summary

The combination of highly charged ions with high-intensity or high photon-energy lasers opens up new opportunities to observe possible new effects or test known effects beyond the laser parameters used by now.

Laser pulses with the properties described in this publication are only delivered by large-scale laser facilities. We have set up a versatile device to produce highly charged ions and prepare them for laser ionisation experiments. The setup is transportable and can be and already has been connected to a laser facility. During commissioning we have produced and captured different ion species, such as C^{2+}, C^{5+} and O^{5+}, reliably.

The ions have been detected non-destructively with a resonant circuit after capturing them in the trap. The vanishing ion signal after six minutes we could assign to ion cooling as the ions were still detectable after 14 minutes.

For detailed investigation of the ion storage time, we have stored the ion for a defined period and analysed the trap content and the number of stored ions destructively. In this course, we have developed a procedure to determine the ion species inside the trap which were produced by charge exchange with the residual gas. This

procedure can also be used to detect single ions produced by laser-ion interaction. We have found hydrogen to be the dominant residual gas and we could determine the background pressure to be around 2×10^{-10} mbar. The determined background pressure was sufficiently low to perform first ion-laser experiments.

We have applied at the FLASH Free-Electron laser-facility for beamtime and seven days of beamtime were granted to investigate the multi-photon ionisation with lithium-like oxygen.

Within two weeks we have been able to install the device at the FLASH laser facility at DESY in Hamburg and brought it back into operation again.

Unfortunately, we have identified a poor background pressure of unknown origin. This limited the storage time of the ions to less than a second for C^{5+}. In consequence, we have decided to use lower charged C^{2+} ions instead and stored them for only a few tens of milliseconds. During this time, the formation of a solid ion cloud has not been possible though, but we have shown the interaction of the carbon ions with the laser.

In future experiments we will have to cope with vacuum conditions present at different laser facilities. That is why we will add a set of apertures to the trap openings. As the laser diameter of the FEL is below 1 mm at this position, this will not interfere with the laser radiation at all. For strongly focussed lasers we design and build a smaller and shorter trap to prevent residual gas from the outside to spoil the interaction region.

In the course of this publication, we have described experiments with highly charged ions with laser radiation at extreme conditions. Apart from the measurements of interest proposed here, the setup allows a broad variety of related experiments due to the versatility of the Penning trap and its related techniques for trapping, selecting and manipulating ions of nearly any charge-to-mass ratio. The limiting factors here are the availability of laser beam time and the initial gases from which the ions are produced. At the moment, we use carbon-dioxide, nitrogen and noble gases up to xenon. Other materials are possible but need further development effort.

We have shown the successful transport, re-installation and operation of the setup at a laser facility. The laser-ion interaction of stored ions has been detected. We have identified the limiting issues and will modify the ion trap accordingly to obtain sufficient long storage times.

Acknowledgments

We acknowledge DESY (Hamburg, Germany), a member of the Helmholtz Association HGF, for the provision of experimental facilities. Parts of this research were carried out at FLASH2 and we would like to thank Marion Kuhlmann for assistance in using the micro-focus FL24 Beamline. We acknowledge Siarhei Dziarzhytski providing the compact spectrometer and Sven Toleikis for general support.

Data availability statement

The data that support the findings of this study are available upon reasonable request from the authors.

ORCID iDs

S Ringleb https://orcid.org/**0000-0002-4957-1635**
M Kiffer https://orcid.org/0000-0002-1356-8653
N Stallkamp https://orcid.org/0000-0003-0588-4207
J Hofbrucker https://orcid.org/0000-0002-5917-3649
B Reich https://orcid.org/0000-0001-7041-8494
G Brenner https://orcid.org/0000-0002-1755-876X
M Ruiz-Lopéz https://orcid.org/**0000-0002-7206-6557**
S Düsterer https://orcid.org/0000-0003-4379-1327
M Vogel https://orcid.org/0000-0002-3768-3293
Th Stöhlker https://orcid.org/0000-0003-0461-3560
G G Paulus https://orcid.org/0000-0002-8343-8811

References

[1] Strickland D and Mourou G 1985 *Opt. Commun.* **55** 447–9
[2] Becker G *et al* 2019 *Sci Rep* **9** 17169
[3] Agostini P, Fabre F, Mainfray G, Petite G and Rahman N K 1979 *Phys. Rev. Lett.* **42** 1127–30
[4] Paulus G G, Nicklich W, Xu H, Lambropoulos P and Walther H 1994 *Phys. Rev. Lett.* **72** 2851–4
[5] Larochelle S, Talebpour A and Chin S L 1998 *J. Phys. B: At. Mol. Opt. Phys.* **31** 1201

[6] L'Huillier A and Balcou P 1993 *Phys. Rev. Lett.* **70** 774–7
[7] Lewenstein M, Balcou Ph, Ivanov M Yu, L'Huillier A and Corkum P B 1994 *Phys. Rev.* A **49** 2117–32
[8] Hornung M *et al* 2016 *Opt. Lett.* **41** 5413–6
[9] Bagnoud V *et al* 2010 *Appl. Phys.* B **100** 137–50
[10] Sävert A, Schäfer G, Beleites B, Ronneberger F, Kaluza M C, Zepf M, Bagnoud V and Stöhlker T 2014 *annual report of the Helmholtz Instutute Jena* **1** 18
[11] Yamakawa K, Akahane Y, Fukuda, Aoyama M, Inoue N, Ueda H and Utsumi T 2004 *Phys. Rev. Lett.* **92** 123001
[12] Ammosov M V, Delone N B and Krainov V P 1986 *Sov. Phys. JETP* **64** 1191–4
[13] Popov V S, Karnakov B M, Mur V D and Pozdyakov S G 2006 *J. Exp. Theor. Phys.* **102** 760–75
[14] Milosevic N, Krainov V P and Brabec T 2002 *Phys. Rev. Lett.* **89** 193001
[15] Ackermann W *et al* 2007 *Nat. Photonics* **1** 336–42
[16] Faatz B *et al* 2016 *New J. Phys.* **18** 062002
[17] Hofbrucker J, Eiri L, Volotka A V and Fritzsche S 2020 *Atoms* **8** 54
[18] Madsen L B and Lambropoulos P 1999 *Phys. Rev.* A **59** 4574
[19] Ghimire S, Fuchs M, Hastings J, Herrmann S C, Inubushi Y and Pines J 2016 *Phys. Rev.* A **94** 043418
[20] Doumy G *et al* 2011 *Phys. Rev. Lett.* **106** 083002
[21] Vorobjev G, Sokolov A, Thorn A, Herfurth F, Kester F O, Quint W, Stöhlker T and Zschornack G 2012 *Rev. Sci. Inst.* **83** 053302
[22] Simon M C *et al* 2010 *Phys. Rev. Lett.* **105** 183001
[23] Vogel M, Quint W, Paulus G G and Stöhlker T 2012 *Nucl. Instr. Meth.* B **285** 65–71
[24] Becker W, Grasbon F, Kopold R, Milošević D B, Paulus G G and Walther H 2002 *Advances In Atomic, Molecular, and Optical Physics* 48 (San Diego: Academic Press Inc.) 35–98
[25] Keldysh L W 1965 *Soviet Physics JETP* **20** 1307–14
[26] Krainov V P 1999 *J. Phys. B: At. Mol. Opt. Phys* **32** 1607–14
[27] Chowdhury E A, Barty C P J and Walker B C 2001 *Phys. Rev.* A **63** 042712
[28] L'Huillier A, Lompre L A, Mainfray G and Manus C 1983 *Phys. Rev.* A **27** 2503–12
[29] Palaniyappan S, Mitchell R, Sauer R, Ghebregziabher I, White S L, Decamp M F and Walker B C 2008 *Phys. Rev. Lett.* **100** 183001
[30] Malmberg J M and O'Neil T M 1977 *Phys. Rev. Lett.* **39** 1333–6
[31] Bharadia S, Vogel M, Segal D M and Thompson R C 2012 *Appl. Phys.* B **107** 1105–15
[32] Bollinger J J, Heinzen D J, Moore F L, Itano W M, Wineland D J and Dubin D H E 1993 *Phys. Rev.* A **48** 525–45
[33] Ringleb S, Vogel M, Kumar S, Quint W, Paulus G G and Stöhlker T 2015 *J. Phys. Conf. Ser.* **635** 092124
[34] Kiffer M, Ringleb S, Stallkamp N, Arndt B, Blinov I, Kumar S, Stahl S, Stöhlker T and Vogel M 2019 *Rev. Sci. Instrum.* **90** 113301
[35] Marshall A G, Hendrickson C L and Jackson G S 1998 *Mass Spectrom. Rev.* **17** 1–35
[36] Guan S and Marshall A G 1993 *Anal. Chem.* **65** 1288–94
[37] Wineland D J and Dehmelt H G 1975 *J. Appl. Phys.* **46** 919–30
[38] Vogel M 2018 *Particle Confinement in Penning Traps* (Switzerland: Springer International Publishing) (https://doi.org/10.1007/978-3-319-76264-7)
[39] Hetzheim H G and Keitel C H 2009 *Phys. Rev. Lett.* **102** 83003
[40] Ye D F, Xin G G, Liu J and He X T 2010 *J. Phys. B: At. Mol. Opt. Phys.* **43** 235601
[41] Bauke H, Hetzheim H G, Mocken G R, Ruf M and Keitel C H 2011 *Phys. Rev.* A **83** 063414
[42] McNaught S J, Knauer J P and Meyerhofer D D 1998 *Phys. Rev.* A **58** 1399–411
[43] Seres J, Seres E, Verhoef A J, Tempea G, Streli C, Wobrauschek P, Yakovlev V, Scrinzi A, Spielmann C and Krausz F 2005 *Nature* **433** 596
[44] Avetissian H K and Markossian A G 2007 *Phys. Rev.* A **76** 053406
[45] LaForge A C *et al* 2021 *Phys. Rev. Lett.* **127** 213202